Structural characterization, thermoluminescence and EPR studies of Nd$_2$O$_3$:Co^{2+} nanophosphors

B. Umesh [a,b], B. Eraiah [b,**], H. Nagabhushana [c,*], S.C. Sharma [c], D.V. Sunitha [c], B.M. Nagabhushana [d], J.L. Rao [e], C. Shivakumara [f], R.P.S. Chakradhar [g,***]

[a] Department of Humanities, PVP Polytechnic, Dr. AIT Campus, Bangalore 560 056, India
[b] Department of Physics, Bangalore University, Bangalore 560 056, India
[c] Prof. C.N.R. Rao Centre for Advanced Materials, Tumkur University, Tumkur 572 103, India
[d] Department of Chemistry, M.S. Ramaiah Institute of Technology, Bangalore 560 054, India
[e] Department of Physics, Sri Venkateswara University, Tirupati 517 502, India
[f] Solid State and Structural Chemistry Unit, Indian Institute of Science, Bangalore 560 012, India
[g] CSIR – National Aerospace Laboratories, Bangalore 560 017, India

A R T I C L E   I N F O

A B S T R A C T

Nd$_2$O$_3$:Co^{2+} (1–4 mol%) nanophosphors (15–25 nm) have been prepared via low temperature solution combustion method. Scanning electron micrograph (SEM) shows that the product is highly porous in nature. The stokes line in the Raman spectrum at ∼2000 cm^{-1} is assigned to F_g mode and the anti-stokes lines are assigned to a combination of $A_g + E_g$ modes. With increase of Co^{2+} concentration, the intensity of F_g mode decreases, whereas the combination of $A_g + F_g$ modes completely disappears. Electron paramagnetic resonance (EPR) spectrum exhibits two resonance signals with effective g values at $g = 2.25$ and $g = 2.03$. Thermoluminescence (TL) response of Nd$_2$O$_3$:Co^{2+} nanopowders with γ dose 0.23–2.05 kGy was studied. The activation energy (E) and frequency factor (s) are estimated using Chen's glow peak shape method and obtained to be in the range 0.45–1.67 eV and 1.8×10^4 to 4.0×10^{12} s^{-1}, respectively. It is observed that the TL glow peak intensity at 430 K increases linearly with γ dose which is suitable for radiation dosimetry.

1. Introduction

Nanotechnology is a growing area of research, primarily due to its numerous applications in engineering/science. Therefore, the synthesis of new nanomaterials and improving its properties are of current research interest to many researchers. It has been found that the physical properties of individual nanoparticles can be very different from those of their bulk counterparts [1]. Rare earth compounds have been extensively used in high performance luminescent devices, magnets, catalysts, and other functional materials because of their electronic, optical and chemical characteristics resulting from the 4f shell of their ions [2–4]. These properties depend strongly on the material composition and structure, which are sensitive to the bonding states of rare earth ions. If the rare earth oxides were fabricated in the form of one dimensional nanostructure, they would have new properties as a result of both their marked shape-specific and quantum confinement effects. They would also act as electrically, magnetically, or optically functional host materials for rare earth ions in phosphor displays, waveguide devices, and for the active material in lasers [5].

Studies on radiation induced defects in insulating materials have been interesting over the last few decades. TL is one such radiation induced defect related process in crystalline materials. In TL, while heating the irradiated material, energy stored in the material is released with the emission of light and the intensity of the emitted light as a function of temperature forms a glow curve. The position, shape and intensity of the glow peaks are related to the properties of the trapping states responsible for TL [6]. The main applications of these materials are in radiation dosimetry for personnel and environmental monitoring, etc. Recent studies on oxide luminescent nanomaterials show that they have a potential application in the radiation dosimetry of high doses of ionizing radiation, where the conventional microcrystalline phosphors saturate [6–8]. This saturation occurs due to the ionized zones overlapping each other in the micro materials at higher doses. However, with the use of very tiny particles such as nanoscale thermoluminescent dosimetry (TLD) materials, this problem is overcome to a major extent [9].

* Corresponding author. Tel.: +91 9945954010.
** Corresponding author. Tel.: +91 9449804014.
E-mail addresses: eraiah@rediffmail.com (B. Eraiah), bhushanvlc@gmail.com (H. Nagabhushana), sreechakra72@yahoo.com (R.P.S. Chakradhar).
*** Corresponding author.

Besides the synthesis of $Nd_2O_3:Co^{2+}$ (1–4 mol%) nanophosphors, this paper also provides a detailed analysis of phosphor using X-ray diffraction (XRD), scanning electron microscopy (SEM), transmission electron microscopy (TEM), Fourier transform infrared spectroscopy, Raman spectroscopy (FTIR), electron paramagnetic resonance (EPR), UV–vis spectroscopy and thermoluminescent techniques. The TL results of the reported nanomaterials have revealed very imperative characteristics such as simple glow peak structure, linear increase in intensity with dose, simple trap distribution. This has encouraged us to study the TL of $Nd_2O_3:Co^{2+}$ nanophosphor using γ irradiation in the dose range 0.23–2.05 kGy.

2. Experimental

2.1. Synthesis of $Nd_2O_3:Co^{2+}$ nanophosphor

An aqueous solution containing stoichiometric amounts of analar grade neodymium nitrate ($Nd(NO_3)_3$; Qualigens Fine chemicals; 99%), cobalt nitrate (Co ($NO_3)_2$; Sigma Aldrich, 99.9%) and oxalyl dihydrazide ($C_2H_6N_4O_2$; ODH) fuel were dissolved in a minimum quantity of double distilled water in a cylindrical Petri dish of 150 ml capacity. ODH was used as a fuel in the combustion synthesis and it is prepared in our laboratory by the reaction of diethyl oxalate ($C_6H_{10}O_4$) and hydrazine hydrate (H_6N_2O) as described in the literature [10]. The mixture was dispersed well using a magnetic stirrer for about 5 min. A petri dish containing the heterogeneous mixture was placed in a pre-heated muffle furnace maintained at $400 \pm 10\ °C$. The reaction mixture initially undergoes thermal dehydration followed by ignition with liberation of large gaseous products such as oxides of nitrogen and carbon. The flame temperature during combustion reaction was measured using an optical pyrometer which is kept inside the furnace. The flame temperature during combustion was found to be $1100\ °C$. The combustion reaction persists for 2–3 min yielding a highly voluminous and foamy product.

The powder X-ray diffraction studies were carried out using Philips X-ray diffractometer (model PW 3710) with CuK_α radiation ($\lambda = 1.5405\ \text{Å}$). The surface morphology of the samples was examined using scanning electron microscopy (JEOL JSM 840A) by sputtering technique with gold as covering contrast material. Transmission electron microscopy (TEM) analysis was performed on a Hitachi H-8100 (accelerating voltage up to 200 kV, LaB_6 filament) equipped with EDS (Kevex Sigma TM Quasar, USA). The UV–vis spectra were recorded on a UV-3101 Shimadzu Visible spectrometer. The EPR spectrum was recorded at room temperature using a JEOL-FE-1X EPR spectrometer operating at the X-band frequency ($\approx$9.205 GHz) with a field modulation frequency of 100 kHz. The magnetic field was scanned from 0 to 500 mT and the microwave power used was 10 mW. A powdered specimen of 100 mg was taken in a quartz tube for EPR measurements. Raman spectroscopic studies were performed on Renishaw In-via Raman spectrometer with 633 nm He–Cd laser and a Leica DMLM optical microscope equipped with $50\times$ objective, thus providing a laser spot of 2 μm in diameter. TL measurements were carried out at room temperature using Nucleonix TL reader using Co^{60} γ-source as excitation in the dose range 0.23–2.05 kGy.

3. Results and discussion

3.1. Structural characterization

Fig. 1(a–d) shows powder X-ray diffraction (PXRD) patterns of Co^{2+} (1–4 mol%) doped Nd_2O_3 phosphor. All the powder diffraction peaks correspond to hexagonal phase with A-type of Nd_2O_3 (JCPDS No. 83-1353). Further, no secondary phase or impurity peaks was
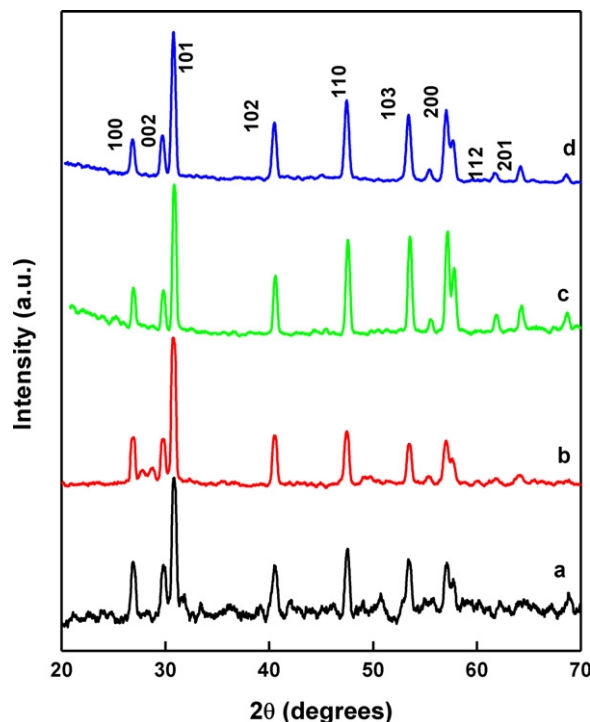

Fig. 1. PXRD patterns of $Nd_2O_3:Co^{2+}$ nanophosphor: (a) 1 mol%, (b) 2 mol%, (c) 3 mol%, (4) 4 mol%.

observed which confirms the phase purity of the sample. The crystallite size was estimated from the broad PXRD peaks using the Scherer's equation [11].

The crystallite size was found to be in the range 15–25 nm. A small shift in the position of main peak (1 0 1) to the lower side of 2θ values. A peak shift in XRD profiles arises due to the presence of size effect or micro strains or presence of both of them [12]. Further, the particle size of Co^{2+} (1–4 mol%) Nd_2O_3 sample was also estimated from the intense Raman line (2000 cm^{-1}) broadening using the equation [13].

$$\Gamma(cm^{-1}) = 10 + \frac{124.7}{D_R} \tag{1}$$

where $\Gamma(cm^{-1})$ is the full-width at half-maximum of the Raman active mode peak and D_R is the particle size of a sample. By substituting $\Gamma(cm^{-1}) = 461\ cm^{-1}$ in the above relation, the particle size of the Nd_2O_3 sample was obtained to be 12 nm. This is in good agreement with Williamson and Hall (W–H) and Scherer's method.

Williamson and Hall suggested a method [14] combining the domain size and lattice micro strain effects on line broadening, when both are operative. The W–H approach considers the case when the domain effect and lattice deformation are both simultaneously operative and their combined effects give the final line broadening FWHM (β), which is the sum of β (grain size) and β (lattice distortion). This relation assumes a negligibly small instrumental contribution compared to the sample-dependent broadening. The strain (ε) and crystallite sizes evaluated from W–H method are listed in Table 1. It is observed that, the strain is more in 3 mol% Co doped sample and it decreases with increase of Co^{2+} (4 mol%) concentration.

Fig. 2 shows the Rietveld refinement performed on the $Nd_2O_3:Co^{2+}$ (3 mol%) nanopowder, which shows highest intensity. The Rietveld refinement is a method in which the profile intensities obtained from step-scanning measurements of the powders allow to estimate an approximate structural model for the real structure. In our work, the Rietveld refinement was performed through the

Table 1

Crystallite size, band gap and strain values in Nd_2O_3:Co^{2+} (1–4 mol%) nanophosphor.

Nd_2O_2:Co^{2+} (mol%)	Band gap (eV)	Particle size (nm)		Strain ($\times 10^{-3}$)
	E_g	Debye–Scherrer's method (d)	W–H method (D)	
1	5.34	15	15	9.83
2	5.38	17	16	14.5
3	5.40	20	18	20.7
4	5.46	18	18	7.81

FULLPROF program [15]. We utilize the psedo-voigt function in order to fit the several parameters to the data point: one scale factor, one zero shifting, four back ground, three cell parameters, five shape and width of the peaks, one global thermal factors and two asymmetric factors. A typical analysis of the Nd_2O_3:Co^{2+} (3 mol%) nanopowder in Fig. 2 presents the experimental and calculated PXRD patterns obtained by the Rietveld refinement. The packing diagram of corresponding Nd_2O_3:Co^{2+} nanopowder after Rietveld refinement was shown in Fig. 3. The refined parameters such as occupancy and atomic functional positions of the Nd_2O_3 nanopowder are summarized in Table 2. The fitting parameters (R_p, R_{wp} and χ^2) indicate a good agreement between the refined and observed PXRD patterns for the Nd_2O_3:Co^{2+} nanopowder.

The surface morphology of Co^{2+} (1–4 mol%) doped Nd_2O_3 nanopowders were studied and SEM images are shown in Fig. 4. It is observed from SEM micrographs that, the crystallites have more porous, agglomeration with irregular morphology. This type of porous network with lot of voids is typical features of combustion synthesis in oxide powders due to escaping gases [16]. The porous powders are highly friable which facilitates easy grinding to obtain finer particles. It is observed from the SEM micrographs that the crystallites have no uniform shape. This is believed to be related to the non-uniform distribution of temperature and mass flow in the combustion flame [17,18]. Further the porosity increases with increase of Co^{2+} concentration. Fig. 5 shows the transmission electron micrograph of Co^{2+} (3 mol%) doped Nd_2O_3 which shows that the crystallites are fused with each other. The average particle size was observed in the range of 15–25 nm. This was also confirmed by Debye–Scherrer's equation and W–H plots. The grain size determined from W–H plots is slightly higher than those calculated using Scherrer's formula (Table 1). The small variation in the values is due to the fact that in Scherrer's formula, strain component is assumed to be zero and observed broadening of
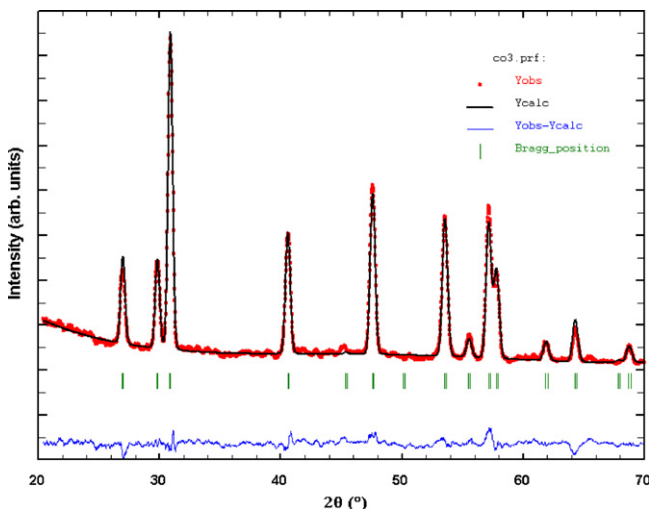

Fig. 2. Rietveld refinement of Nd_2O_3:Co^{2+} (3 mol%) nanophosphor.

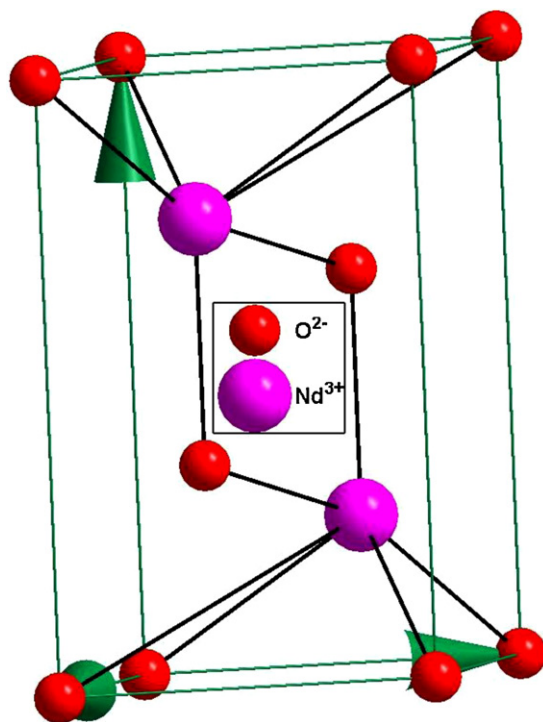**Fig. 3.** Packing diagram of Nd_2O_3:Co^{2+} (3 mol%) nanophosphor.

diffraction peak is considered as a result of reducing grain size only. Further, it is observed that the strain for 3 mol% Co^{2+} doped sample is greater than that of 1, 2 and 4 mol% Co^{2+}. This increase in strain causes the broadening and shift in XRD peaks in Co doped sample.

Fig. 6 shows the FTIR spectra of Nd_2O_3:Co^{2+} (1–4 mol%) phosphor. The peaks at 407 and 670 cm^{-1} are the characteristic metal–oxygen (Nd–O) vibrations. A sharp peak at 3615 cm^{-1} represents M–OH peak. The band between 3500 and 3800 cm^{-1} is due to the (O–H) vibration of H_2O absorbed by Nd_2O_3 phosphor. The band between 1350 and 1500 cm^{-1} is assigned to the carbonate peaks and these bands are observed in all the samples. Fig. 7 shows the Raman spectra of Nd_2O_3:Co^{2+} (1–4 mol%) nanophosphors recorded at room temperature with an excitation wavelength of 633 nm He–Cd laser. It is a nondestructive and potential probe for investigating the structural properties of nanomaterials [19]. Different features were observed with increase of Co^{2+} dopant namely (i) broadening of the intense Raman line, (ii) shift of the Raman peak positions and (iii) change in intensity of the Raman peaks. A strong Raman peak (Stokes line) at 2000 cm^{-1}a-1along with weak peaks (anti stokes) at 1442, 1629, 1840, 1942, 2061, 2109 cm^{-1} was observed up to 3 mol% Co^{2+} concentration. The strong and intense peak at 2000 cm^{-1} has been assigned to F_g mode and other weak peaks at 1442 cm^{-1}, 1629 cm^{-1}, 1840 cm^{-1},

Table 2

Rietveld refinement parameter of Nd_2O_3:Co^{2+} doped (3 mol%) nanophosphor.

Atoms	Oxidation state	Wyckoff notation	Positional parameters			Occupancy
			x	y	z	
Nd_1	3	2d	0.3333	0.6667	0.2482 (2)	0.97
Co	2	2d	0.3333	0.6667	0.2482 (2)	0.03
O_1	2	1a	0.0000	0.0000	0.0000	1.00
O_2	2	2d	0.3333	0.6667	0.6474 (5)	1.00

Crystal system = Hexagonal.
Lattice parameter, a = 3.821 (2) Å, C = 5.996 (3) Å, volume = 75.82 (6) Å^3.
Space group = P-3m1 (164).
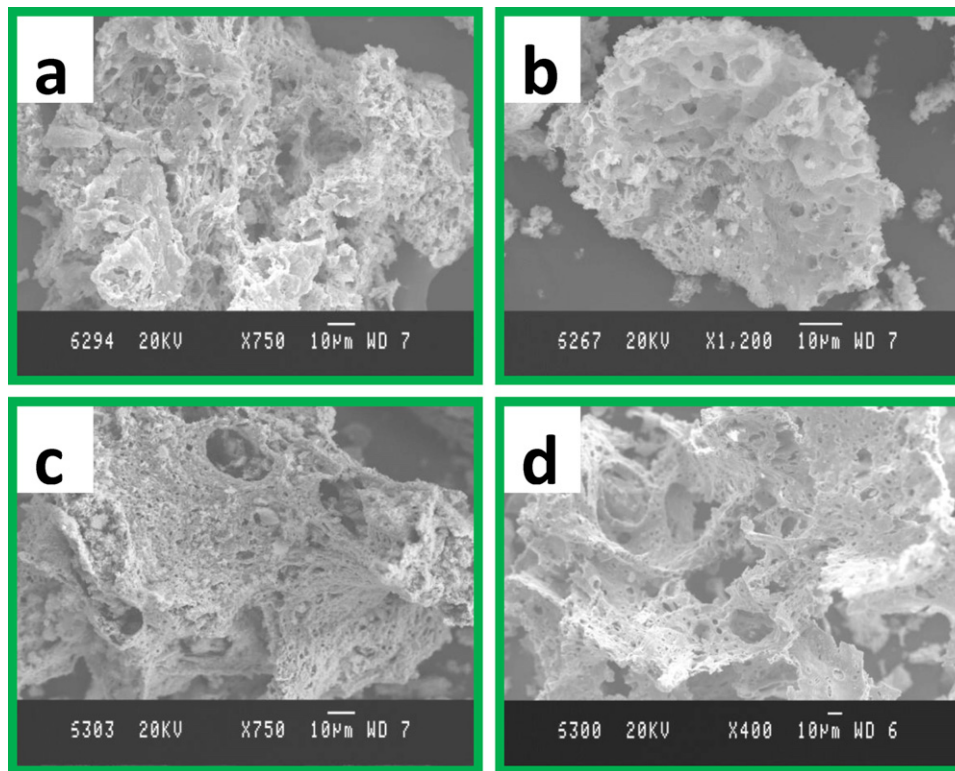$R_{factors}$: R_p = 7.35, R_{wp} = 10.2, R_{Bragg} = 5.62, R_F = 4.57.

Fig. 4. SEM images of $Nd_2O_3:Co^{2+}$ nanophosphor: (a) 1 mol%, (b) 2 mol%, (c) 3 mol%, (4) 4 mol%.

$1942 \, cm^{-1}$, $2061 \, cm^{-1}$, $2109 \, cm^{-1}$ are assigned to combination of F_g and E_g modes. The strong Raman intensity for $2000 \, cm^{-1}$ band indicates a large polarizability change during the vibration. Therefore this band is expected to be more sensitive to changes in chemical bonding. It is observed that the intensity of the Stokes and anti-stoke lines decreases with increase of Co^{2+} concentration (inset of Fig. 7). Further, it is observed that, with increase of Co^{2+} concentration the intense peak ($2000 \, cm^{-1}$) shifted towards lower wavenumber and for higher concentration of Co^{2+} (4 mol%), the peaks at $\sim 1838 \, cm^{-1}$, $2055 \, cm^{-1}$ and $2105 \, cm^{-1}$ completely vanishes.

Many authors [20,21] reported that broadening of the Raman lines in rare earth oxides is due to thermal agitation. It is well known that in the case of nano systems, the Raman frequency undergoes a red shift with a decrease in the radius of the nano solid. Pan et al. [22] suggested that this red shift arises from the cohesive bond weakening of the lower co-ordinated atoms near the surface region of the nanograin. Another factor responsible for the shift may be the short range interactions between a phonon and photon, which describe the covalent bonding and thus are correlated to bond energy and bond length. Another factor governing this shift may be that when the size is decreased, the
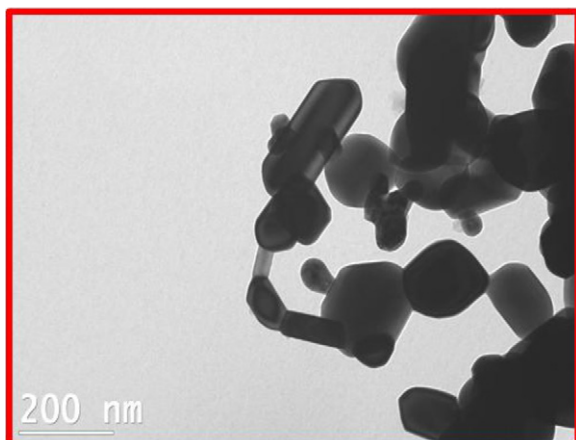

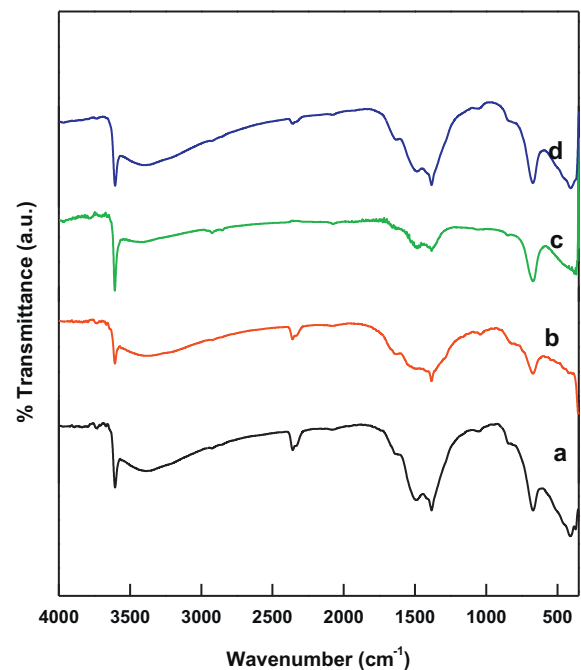**Fig. 5.** TEM picture of $Nd_2O_3:Co^{2+}$ (3 mol%) nanophosphor.

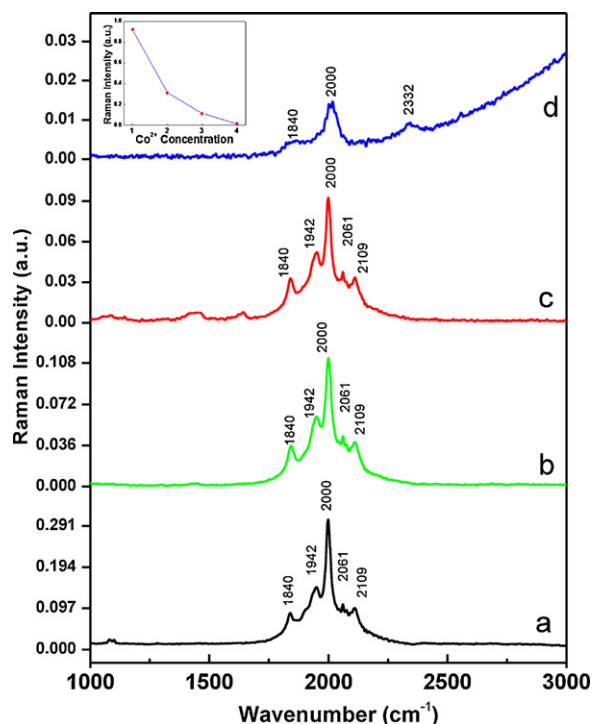**Fig. 6.** FTIR spectra of $Nd_2O_3:Co^{2+}$ nanophosphor (a) 1 mol%, (b) 2 mol%, (c) 3 mol%, (4) 4 mol%.

Fig. 7. Raman spectra of Nd_2O_3:Co^{2+} nanophosphor: (a) 1 mol%, (b) 2 mol%, (c) 3 mol%, (4) 4 mol% (inset: variation of Raman peak intensity at 2000 cm^{-1} vs Co^{2+} concentration).

momentum conservation will be relaxed and the Raman active modes will not be limited at the center of the Brillounin zone.

The UV–visible absorption spectra of different Co^{2+} (1–4 mol%) doped Nd_2O_3 phosphor are shown in Fig. 8. The spectra exhibit a broad and prominent absorption band with a maximum at ~226–240 nm along with weak absorption bands at ~292 nm. The maximum absorption arises due to transition between valence band to conduction band. The weak absorption in the UV–visible region is expected to arise from transitions involving extrinsic states such as surface traps or defect states or impurities [23]. Smaller size particles are found to have high surface to volume
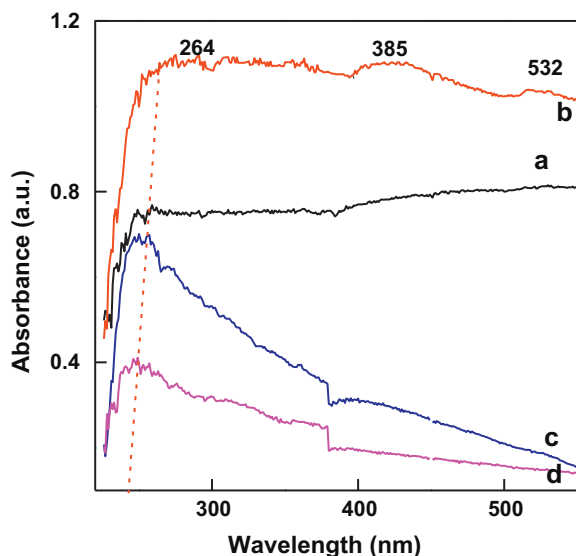

Fig. 8. UV–vis spectra of Nd_2O_3:Co^{2+} nanophosphor: (a) 1 mol%, (b) 2 mol%, (c) 3 mol%, (4) 4 mol%.

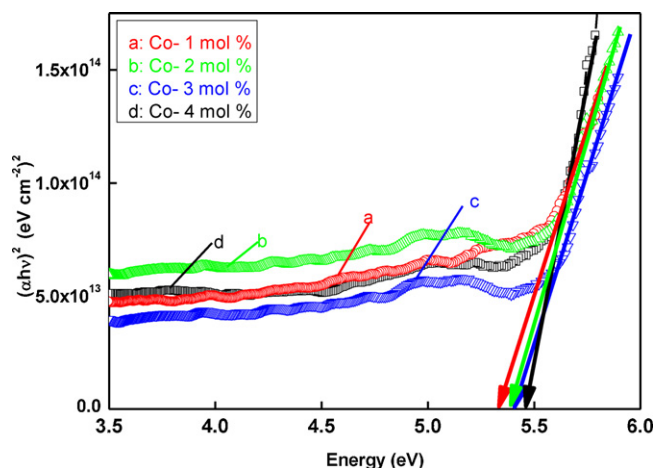**Fig. 9.** Band gap of Nd_2O_3:Co^{2+} nanophosphor: (a) 1 mol%, (b) 2 mol%, (c) 3 mol%, (4) 4 mol%.

ratio. This results in increase of defects distribution on the surface of nanomaterials. Thus the lower is the particle size, the nanomaterials exhibit strong and broad absorption bands [24].

The optical band gap energy (E_g) of Co^{2+} (1–4 mol%) doped Nd_2O_3 phosphor was estimated by Wood and Tauc relation [25] and shown in Fig. 9. The E_g values for different Co^{2+} (1–4 mol%) in Nd_2O_3 phosphor is found to be in the range 5.34–5.46 eV. The value obtained for 3 mol% Co^{2+} is well agreement to those reported in the literature [26]. Further, the E_g values are lesser for 1, 2 mol% Co^{2+} whereas for 4 mol% Co^{2+}, the E_g value is enhanced. The variation in band gap values in 1, 2, and 4 mol% Co^{2+} can be related to the degree of structural order-disorder in the lattice which is able to change the intermediately energy level distribution within the band gap. This is attributed to particle size effect. The nanomaterials have large surface to volume ratio as a result the formation of voids on the surface as well as inside the agglomerated particles. Such voids can cause fundamental absorption in the UV wavelength range [27]. When 3 mol% Co^{2+} doped into Nd_2O_3 matrix it becomes more ordered structure with less defects. Consequently intermediate energy levels (deep and shallow holes) are minimized within the optical band gap. Further, the E_g values depends on various factor the preparation methods and different experimental conditions. In particular these key factors can favor or inhibit the formation of structural defects, which are able to control the degree of structural order–disorder of the material and consequently the number of intermediately energy levels within the band gap.

The EPR spectrum of Nd_2O_3:Co^{2+} (4 mol%) nanopowder at room temperature is shown in Fig. 10. The EPR spectrum of Co^{2+} ions in general is observed only at low temperature because the spin lattice relaxation time is extremely short for Co^{2+} ions. At higher temperature the spectrum become broader probably due to short relaxation time characteristic of high spin state of the Co^{2+} ion [28]. The Co^{2+} with d^7 electron configuration and ^4F ground state has seven fold orbital degeneracy. The ^4F state of d^7 ions in octahedral field splits to ^4T triplet ground state. Spin–orbital interaction leads to splitting of this triplet so that the lowest state is Kramers doublet with isotropic $g = 4.3$. The fields of lower symmetry mix this state with nearly lying excited states, and g-value becomes anisotropic [29]. Therefore the g values become anisotropic and are sensitive to variations in crystal field [30]. While Co^{2+} ions at the tetragonal sites in the lattice should produce a single EPR line with the Lorentzian line shape with a g-factor of ~2.25 [31]. In the present work, the EPR spectrum of Co^{2+} ions in Nd_2O_3 nanopowder exhibit resonance signals with anisotropic g values at $g = 2.25$ and
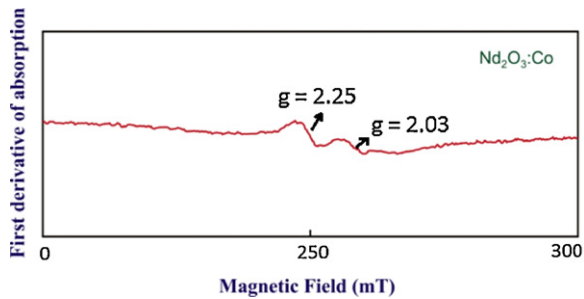
Fig. 10. EPR spectrum of $Nd_2O_3:Co^{2+}$ (4 mol%) nanopowder at room temperature.

$g = 2.03$. These two resonance signals are attributed to Co^{2+} ions at the cubic sites of Nd_2O_3 lattice.

TL measurements probe a class of defects with energy levels in the band gap of insulating/semiconducting materials. Fig. 11 shows the TL glow curves of different concentration of Co^{2+} (1-4 mol%) in Nd_2O_3 host irradiated with 1.14 kGy. Here all the measurements were carried out at room temperature at a constant heating rate $5\,°C\,s^{-1}$. The TL intensity is found to be highest for 3 mol% of Co^{2+}. Fig. 12 shows the TL spectra for optimized concentration of Co^{2+} ions (3 mol%) in Nd_2O_3 nanophosphor irradiated with γ-rays in the dose range 0.23–2.05 kGy. Well resolved glow peaks at 430 K along with shoulder peaks in the range 150–250 K were observed.

The variation of TL glow peak intensity (430 K) with accumulated dose was studied and is shown in Fig. 13. It is observed that the TL intensity increases linearly with increasing γ-dose. This linear behavior of the nanophosphor is highly useful for dosimetric application. Further, it is noticed that there is slight shifting in the glow peak positions to lower temperature side with increase of γ dose. The appearance of more than one TL peak indicates that there are possibly different kinds of trapping centers generated due to γ irradiation. The shallow trapping center leads to the resolved peak at lower temperature and the other deeper center gives rise to shouldered peak at higher temperature. The intensity of the higher temperature glow peak increases linearly with dose. This might be due to high surface to volume ratio, which results in a higher surface barrier energy for the nanoparticles. On increasing the dose, the energy density crosses the barrier and a large number of defects are produced in the nanoparticles which ultimately keep on increasing with the dose till saturation is achieved [32].
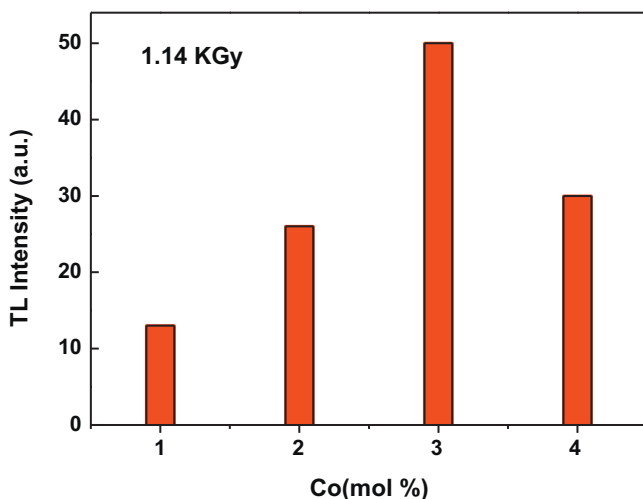

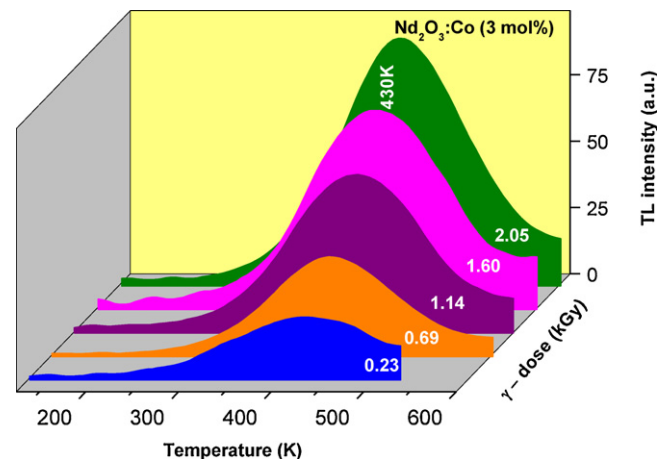Fig. 12. TL glow curves of $Nd_2O_3:Co^{2+}$ (3 mol%) γ-irradiated for: (a) 0.23 Gy, (b) 0.69 Gy, (c) 1.14 kGy, (d) 1.6 kGy, (e) 2.05 kGy.

It is also observed that for lower dosed samples the traps/defects generated appear to be very less due to less surface barrier energy. Hence the glow curve has minimum TL intensity. As the temperature increases, the surface barrier energy also increases. The increase in TL intensity with dose can be explained on the basis of track interaction model [33,34]. According to this model, the number of traps generated by the high energy radiation in a track depends upon the cross section and the length of the track inside the matrix. In the case of nanomaterials, the length of the track generated by high energy radiation is of few tenths of nanometers. At low doses, there exist a few trap centers or luminescent centers owing to the small size of the particles. As the dose increases, the TL intensity increases as the cross section would increase with increase in γ-dose.

In our earlier work [35], $Nd_2O_3:Eu^{3+}$ nanophosphor γ irradiated for 100–400 Gy show well resolved glow peak at ~426 K at a warming rate of $5\,°C\,s^{-1}$. The TL intensity of the sample follows a linear relation with increasing dose. Strong fading was recorded initially after four days; the decay is quite slow and finally stabilizes after 21 days. Soliman [36] observed three glow peaks in the range 310–385 °C in as received Nd_2O_3 powder procured from sigma Aldrich company. However, in heat treated samples show four TL glow curves in the range 170–386 °C at a dose rate of
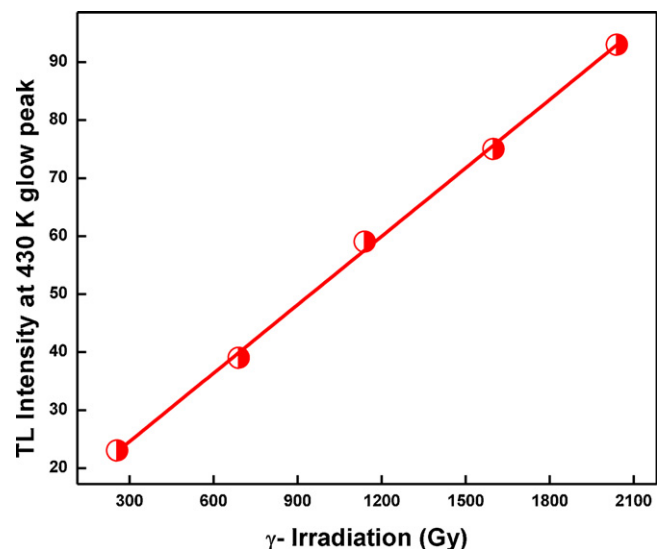

Fig. 11. Variation of TL intensity with of $Nd_2O_3:Co^{2+}$: (a) 1 mol%, (b) 2 mol%, (c) 3 mol%, (d) 4 mol%.

Fig. 13. Variation of TL intensity with γ dose in $Nd_2O_3:Co^{2+}$ (3 mol%).

Table 3
Kinetic parameters of $Nd_2O_3:Co^{2+}$ (1–4 mol%) estimated using Chen's glow peak shape method.

γ-Dose (kGy)	Peak	T_m (K)	Order of kinetics b (μ_g)	Activation energy (eV)				Frequency factor (s^{-1})
				E_τ	E_δ	E_ω	E_{ave}	
2.05	1	334	2 (0.51)	0.738	0.829	0.787	0.785	2.1E+07
	2	400	2 (0.50)	1.010	1.101	1.060	1.057	5.8E+08
	3	444	2 (0.50)	1.121	1.210	1.170	1.167	1.1E+09
	4	501	2 (0.49)	1.207	1.309	1.263	1.259	1.0E+09
1.6	1	320	2 (0.52)	0.637	0.732	0.688	0.686	3.8E+06
	2	369	2 (0.51)	1.353	1.388	1.377	1.372	6.2E+11
	3	433	2 (0.50)	0.997	1.096	1.051	1.048	1.9E+08
	4	507	2 (0.51)	1.651	1.679	1.673	1.667	5.1E+11
1.14	1	337	2 (0.52)	0.388	0.520	0.457	0.455	1.8E+04
	2	417	2 (0.51)	0.852	0.958	0.908	0.906	2.3E+07
	3	482	2 (0.49)	1.712	1.761	1.746	1.740	4.0E+12
	4	558	2 (0.49)	1.088	1.221	1.157	1.155	5.0E+07
0.69	1	325	2 (0.49)	0.649	0.757	0.704	0.703	4.8E+06
	2	395	2 (0.49)	0.944	0.928	0.882	0.918	5.2E+07
	3	439	2 (0.51)	1.322	1.126	1.108	1.185	1.7E+09
	4	496	2 (0.50)	1.492	1.159	1.134	1.262	1.2E+09
0.23	1	331	2 (0.48)	0.920	0.590	0.550	0.687	2.0E+06
	2	408	2 (0.52)	1.140	0.601	0.582	0.774	2.2E+06
	3	414	2 (0.49)	0.984	0.375	0.329	0.563	4.3E+04
	4	482	2 (0.49)	1.835	0.969	0.958	1.254	1.6E+09

600 Gy.The variation in TL glow peak temperature and the number of glow peaks in present study might be due to particle size effect, method of preparation of the phosphor, heating rate, type of ionizing radiation [37].

The dosimetric properties of TL materials depend on the kinetic parameters of its glow peak. Kinetic parameters give valuable information about mechanism responsible for the emission in material. Reliable dosimetric studies of any TL material include a good knowledge of its kinetic parameters well. The important kinetic parameters are trap depth or activation energy (E) which is the thermal energy required to liberate the trapped electrons and holes, frequency factor (s) and the order of kinetics (b). These parameters can be estimated using Chen's set of empirical equations [38].

Further, activation energy (E) and frequency factor can also be estimated using Chen's peak shape method [38]. The trapping parameters (E, b, s) estimated for different γ-doses are given in Table 3.

4. Conclusions

Different concentrations of Co^{2+} doped Nd_2O_3 nanophosphor have been synthesized by solution combustion method for the first time using oxalyl dihydrazide ($C_2H_6N_4O_2$; ODH) as a fuel. XRD patterns confirm that hexagonal (A-type) phase without impurity peaks. TEM and XRD studies showed that crystallite size were nanocrystalline in nature. Rietveld refinement confirmed the space group of the structure to be P-3m1 (164) with lattice parameter $a = 3.821$ (2) Å, $c = 5.996$ (3) Å and cell volume (V) = 75.82 (6) Å^3. The electronic band gap of $Nd_2O_3:Co^{2+}$ (1–4 mol%) estimated from UV–Vis spectroscopy is in the range 5.34–5.46 eV. Two resonance signals with g-values at 2.25 and 2.03 and are attributed to Co^{2+} ions. A well resolved TL glow peak at 430 K along with shouldered peaks in the range 150–250 K was observed at a warming rate of $5 °C s^{-1}$. TL intensity of the glow peak at 430 K increases linearly with the increase of γ dose. Simple glow peak shape, simple trap distribution, linear increase in TL intensity with increase of γ dose which make $Nd_2O_3:Co^{2+}$ (3 mol%) nanophosphor might be used in radiation dosimetry.

References

[1] L.V. Interrante, M.J. Hampden-Smith, Chemistry of Advanced Materials: An Overview, Wiley VCH, New York, 1998.
[2] X. Qu, J. Dai, J. Tian, X. Huang, Z. Liu, Z. Shen, P. Wang, J. Alloys Compd. 469 (2009) 332–335.
[3] L. Qian, Y. Gui, S. Guo, Q. Gong, X. Qian, J. Phys. Chem. Solids 70 (2009) 688–693.
[4] R. Bazzi, M.A. Flores-Gonzalez, C. Louis, K. Lebbou, C. Dujardin, A. Brenier, W. Zhang, O. Tillement, E. Bernstein, J. Lumin. 445 (2003) 102–103.
[5] A.G. Dedov, A.S. Loktev, I.I. Moiseev, A. Aboukais, J.F. Lamonier, I.N. Filimonov, Appl. Catal. A 245 (2003) 209–220.
[6] J. Azorin, Nucl. Tracks Rad. Meas. 11 (1986) 159–166.
[7] G. Kitis, C. Furetta, M. Prokic, V. Prokic, J. Phys. D: Appl. Phys. 33 (2000) 1252–1262.
[8] P.D. Sahare, R. Ranjan, N. Salah, S.P. Lochab, J. Phys. D 40 (2007) 759–764.
[9] S.P. Lochab, P.D. Sahare, R.S. Chauhan, N. Salah, A. Pandey, J. Phys. D 40 (2007) 1343–1350.
[10] B.M. Nagabhushana, Ph.D. Thesis, Bangalore University, 2008.
[11] P. Klug, L.E. Alexander, X-ray Diffraction Procedure, Wiley, New York, 1954.
[12] S. Ekambaram, Y. Iikubo, A. Kudo, J. Alloys Compd. 433 (2006) 237–240.
[13] Z. Wang, Z. Quan, J. Lin, Inorg. Chem. 46 (13) (2007) 5237–5242.
[14] G.K. William, W.H. Hall, Acta Metall. 1 (1953) 22–31.
[15] R.W.G. Wyckoff, Crystal Structures, vol. 2, Interscience, New York, 1964, pp. 4–5.
[16] A. Jagannatha Reddy, M.K. Kokila, H. Nagabhushana, R.P.S. Chakradhar, C. Shivakumara, J.L. Rao, B.M. Nagabhushana, J. Alloys Compd. 509 (2011) 5349–5355.
[17] B. Nagappa, G.T. Chandrappa, Microporous Mesoporous Mater. 106 (2007) 212–218.
[18] K.C. Patil, M.S. Hegde, S.T. Aruna, T. Rattan, Chemistry of Nanocrystalline Oxide Materials, Combustion Synthesis, Properties and Applications, World Scientific Publishing Co. Pvt. Ltd., UK, 2008.
[19] A. Jagannatha Reddy, M.K. Kokila, H. Nagabhushana, J.L. Rao, C. Shivakumara, B.M. Nagabhushana, R.P.S. Chakradhar, Spectrochim. Acta A 81 (2011) 53–58.
[20] W.B. White, V.G. Keramidas, Spectrochim. Acta A 28 (1972) 501–509.
[21] W. Urben Marek, C. Cornilsen Bahn, J. Phys. Chem. Solids 48 (1984) 475–480.
[22] L.K. Pan, C.Q. Sun, C.M. Li, J. Phys. Chem. B 108 (2004) 3404–3406.
[23] H.Q. Cao, X.Q. Qiu, B. Luo, Y. Liang, Y.H. Zhang, R.Q. Tan, M.J. Zhao, Q.M. Zhu, Adv. Funct. Mater. 14 (2004) 243–246.
[24] A. Emeline, G.V. Kataeva, A.S. Litke, A.V. Rudakova, V.K. Ryabchuk, N. Serpone, Langmuir 14 (1998) 5011–5022.
[25] J. Tauc, in: F. Abeles (Ed.), Optical Properties of Solids, North-Holland, Amsterdam, 1970.

[26] B. Umesh, B. Eraiah, H. Nagabhushanac, B.M. Nagabhushana, G. Nagaraja, C. Shivakumara, R.P.S. Chakradhar, J. Alloys Compd. 509 (2011) 1146–1151.

[27] N. Salah, S.S. Habib, Z.H. Khan, S.A. Hamedi, S.P. Lochab, J. Lumin. 129 (2009) 192–196.

[28] F. Gan, H. Deng, H. Liu, J. Non-Cryst. Solids 52 (1982) 143–149.

[29] S. Ruck, D. Stachel, Phosphorus Res. Bull. 13 (2002) 201–204.

[30] A. Abragam, B. Bleaney, Electron paramagnetic resonance of transition ions, Oxford University Press, 1970.

[31] S. Angelov, E. Zhecheva, R. Stoyanova, M. Atanasov, J. Phys. Chem. Solids 51 (1990) 1157–2116.

[32] M. Chandrasekhar, D.V. Sunitha, N. Dhananjaya, H. Nagabhushana, S.C. Sharma, B.M. Nagabhushana, C. Shivakumara, R.P.S. Chakradhar, J. Lumin. 132 (2012) 1798–1806.

[33] S. Mahajna, Y.S. Horowitz, J. Phys. D: Appl. Phys. 30 (1997) 2603–2619.

[34] Y.S. Horowitz, O. Avila, M. Rodrigues-Villafuerte, Nucl. Instrum. Methods Phys. Res. B 184 (2001) 85–112.

[35] B. Umesh, B. Eraiah, B.M. Nagabhushana, H. Nagabhushana, H.B. Premkumar, C. Shivakumara, C.H. Rayappa, R.P.S. Chakradhar, Phil. Mag. Lett. 89 (2009) 589–597.

[36] C. Soliman, Nucl. Instrum. Methods B 251 (2006) 441–444.

[37] H. Nagabhushana, Ph.D. Thesis, Bangalore University, 2003.

[38] R. Chen, S.W.S. Mckeever, Theory of Thermoluminescence and Related Phenomena, World Scientific Press, Singapore, 1997.